

Eigen-Factors an Alternating Optimization for Back-end Plane SLAM of 3D Point Clouds

Gonzalo Ferrer¹, Dmitrii Iarosh², Anastasiia Kornilova¹

Abstract—Modern depth sensors can generate a huge number of 3D points in few seconds to be latter processed by Localization and Mapping algorithms. Ideally, these algorithms should handle efficiently large sizes of Point Clouds under the assumption that using more points implies more information available. The Eigen Factors (EF) is a new algorithm that solves SLAM by using planes as the main geometric primitive. To do so, EF exhaustively calculates the error of all points at complexity $O(1)$, thanks to the *Summation matrix* S of homogeneous points.

The solution of EF is highly efficient: i) the state variables are only the sensor poses – trajectory, while the plane parameters are estimated previously in closed form and ii) EF alternating optimization uses a Newton-Raphson method by a direct analytical calculation of the gradient and the Hessian, which turns out to be a block diagonal matrix. Since we require to differentiate over eigenvalues and matrix elements, we have developed an intuitive methodology to calculate partial derivatives in the manifold of rigid body transformations $SE(3)$, which could be applied to unrelated problems that require analytical derivatives of certain complexity.

We evaluate EF and other state-of-the-art plane SLAM back-end algorithms in a synthetic environment. The evaluation is extended to ICL dataset (RGBD) and LiDAR KITTI dataset. Code is publicly available at <https://github.com/prime-slam/EF-plane-SLAM>.

Index Terms—SLAM, Plane SLAM, Planar Bundle Adjustment, Differentiation in $SE(3)$.

I. INTRODUCTION

THE advent of modern sensing capabilities is offering the possibility to perceive 3D depth, i.e. Point Clouds (PC), at a high streaming rate from diverse sensors, such as 3D LiDARs, Time of Flight cameras, RGB-D, etc. The more points are used, the more information is gathered from the environment. However, is it possible to evaluate all observed points and improve accuracy without a considerable increase in complexity? This is the main question this paper tries to address.

Aligning a sequence of observed PCs can be formulated as a Simultaneous Localization and Mapping (SLAM) [1] problem, where full trajectory and map geometry are purely estimated from the sensor’s observed 3D points. Similarly, this problem definition fits perfectly the Bundle Adjustment (BA) [2] problem. In this paper, we are interested in the design and study of a new observation function that allows to formulate the SLAM (or BA) problem by directly considering the sensor’s observed points in an efficient manner.

¹The authors with the Skolkovo Institute of Science and Technology (Skoltech), Center for AI Technology (CAIT). [g.ferrer](mailto:g.ferrer@skoltech.ru), anastasiia.kornilova@skoltech.ru.

²The author is with the Software Engineering Department, Saint Petersburg State University.

An important hindrance is that the sensor’s points from PCs are sampled from the scene geometry, consequently it is highly unlikely to observe the same exact point on later observations. Therefore, one needs to define some representation of this inherent geometry that is capable of providing the error-point in an efficient manner. We will choose planar surfaces as landmarks due to their regularity and simple constrain equation. These geometrical surfaces are commonly present in indoors and urban areas. Plane SLAM [3], [4] approaches use planes as landmarks, but the observations are pre-processed into planar features, hence, 3D points are not directly used with their consequent performance deterioration.

We propose a plane SLAM technique for back-end optimization, the Eigen-Factors (EF), tailored for 3D Point Clouds (PC) from RGBD and LiDAR, while being capable of processing a large amount of points with constant complexity. This paper is an improved version of the former EF [5], overcoming its main limitation (first order optimization). The EF uses planar geometric constraints for the alignment of a trajectory described by a moving sensor. To do so, EF aggregates all observed points into the *Summation matrix* S , a summation of outer product of homogeneous points and directly calculates the exact point error at $O(1)$ complexity.

In addition, EF optimizes the point to plane error w.r.t. the trajectory. The plane variables are calculated in closed form in an early step and the resultant problem is an alternating optimization.

The gradient and the Hessian are directly calculated by reformulating the problem in terms of manifold optimization on $SE(3)$ and retractions. Unfortunately, EF does not allow for the Gauss-Newton optimization approximation, since there are not residuals but eigenvalues, so instead we use the Newton-Raphson optimization. In order to differentiate over $SE(3)$, we have proposed a methodology which greatly simplifies the calculation of derivatives of any order and it could be used on other problems where an analytical expression is hard to derive, as in our case through eigenvalues or matrix elements. For our particular configuration, the resulting Hessian is block diagonal which has an impact on the optimization process, since its inversion is extremely efficient.

The contributions of the Eigen Factors are the following:

- Matrix summation S to calculate all point to plane errors at $O(1)$ complexity;
- Alternating optimization where first the plane parameters are calculated in closed form and then the reduced dimensionality problem (only trajectory) is estimated by Newton-Raphson;
- Efficient second order optimization of EF with analytical calculation of the gradient and the Hessian (block

diagonal).

- Methodology to calculate derivatives of any function involving the manifold of rigid body transformations $SE(3)$;

The evaluation compares EF with other state-of-the-art plane SLAM back-end algorithms in synthetic, RGBD and LiDAR environments, since we believe these are the most useful settings for plane SLAM. In order to clearly understand all the details of each method, we have decided to compare only the back-end and provide to all methods the same exact input. The front-end has an impact to the final performance of the methods so we have decided to isolate this effect.

The ideal application of EF is map refinement of 3D PC by optimizing the plane error over trajectories.

II. RELATED WORK

The initial motivation for EF is to align PC minimizing the point error. The Iterative Closest Point (ICP) algorithm [6]–[9] fits a pair of PCs by iteratively finding correspondences and solving the optimization problem [10]–[12]. Existing solutions include matching point-to-point, point-to-line [13], point-to-plane, and other variants emulating planes [14], [15] or assuming a general geometry. These techniques require to process all points every iteration and can achieve high accurate results.

One can bring this idea to a sequence of PC or Multi-view registration. An early work [16] proposed to match all points in every view, reducing the overall point error, but requiring huge memory resources and intense computations. Improvements on Multi-view registration targeted efficiency, for instance considering pairs of PC as constraints [17].

Although computing the overall point error is a natural choice for mapping and SLAM, researchers have been trying to reduce the *a priori* high computational requirements of these techniques. On this regard, processing plane landmarks for each PC observation could be seen as a proxy for computing the point error but at a reduced computational cost. Therefore, plane Landmark-based SLAM optimizes trajectory and a map of plane-landmarks [3], [4]. There have been proposed multitude of variants, some of them focusing on the plane representation [18], [19], adding planar constraints [20] or a mixture of points and planes [21], [22]. The key problem of plane landmarks is that after extracting planar features from noisy points, there is an inevitable loss of information compared to considering jointly all points. EF on the other hand, keeps all points’ information.

Modern mapping approaches, in order to ensure real-time (or close) conditions, aggregate observations to the map after an accurate scan-to-map, effectively marginalizing poses. Examples of these approaches include LOAM [23], [24] which combines PC alignment with mapping or LIO-mapping [25]. Surfel-based approaches [26], [27] follow the same principle dividing the scene in planar disks, obtaining impressive results. When considering loop closure, pure mapping approaches present limitations and require an extra effort to update their mapping solutions properly. SLAM approaches do not suffer this limitation, since in general both the trajectory and the map

are estimated simultaneously, so they handle more naturally loop closure situations at the cost of higher computational resources.

When considering overall point error, efficiency is of the essence. Our previous paper on EF [5] introduces for the first time the S matrix as a summation of outer products the homogeneous points from each sensor pose. This allows to optimize the point to plane error with complexity $O(1)$, which is the key requirement for our approach to work efficiently. Later, π -LSAM [28] makes use of the same matrix S to calculate the overall point to plane error to solve the Planar Bundle adjustment estimating jointly poses and plane-landmarks. In a later work, the authors refer to this homogeneous summation matrix S as the *Integrated Cost Matrix* (ICM) [22].

The BAREG [29] algorithm updates incrementally a covariance matrix 3×3 , without explicit re-evaluation of points, maintaining the same advantages as the S matrix. BALM2 [30] uses the same concept of the S matrix, which is referred there as *Cluster Points* and formalizes some properties of the S matrix such as superposition and transformation.

The idea of using the eigendecomposition from EF as an objective function is adopted by BALM [31], whose derivation is from a 3×3 covariance instead of the 4×4 homogeneous S matrix as in EF. The authors improve the efficiency [30] by calculating analytical derivatives of the gradient and Hessian, in the same spirit we propose in this paper. The derivations are however different: BALM’s Hessian is dense whereas our derivation results in a block diagonal Hessian.

In BAREG [29], the authors use the eigendecomposition to demonstrate the equivalence of the point-to-plane error to the plane-to-plane error, with proper weights. This equivalence assumes that the plane parameters are optimal which might be a too restrictive condition in practice. However, this reduction greatly reduces the complexity and efficiency of the optimization step. It also requires the plane estimation at each observation, which has consequences when evaluating under strong point noise conditions.

In this work, we are interested also in assessing the quality of the map by using a mapping metric. The ground truth on some datasets will not be accurate enough for the mapping purposes, so these assessment tools are necessary. Whereas there are many solutions for precise trajectory estimation from sequences of point clouds, the topic of measuring map quality has not received the same attention. The 3D graphics community proposes a set of full reference metrics for solving tasks of point cloud compression and denoising, including p2point metric, p2plane metric [32], angular similarity [33], projection based methods [34] or SSIM [35], [36]. The majority of metrics based on point cloud requires reference to ground truth, whereas in the evaluation scenario we propose (KITTI), 3D reconstruction ground truth will not be available. Therefore no-reference evaluation is used in this work. In particular, Mean Map Entropy (MME) [37] and Mean Plane Variance (MPV) [38] evaluate noise in the aggregated point cloud and Mutually Orthogonal Metric (MOM) [39] correlates reconstruction noise with perturbation in the 3D poses.

III. EIGEN-FACTORS: POINT TO PLANE ERROR

A plane π in the 3D space is defined by a normal unit vector $\eta \in \mathbb{S}^2$ and the plane distance to the origin $d \in \mathbb{R}$:

$$\pi = \begin{bmatrix} \eta \\ d \end{bmatrix} \in \mathbb{P}^3, \quad \text{where } \|\eta\| = 1. \quad (1)$$

A point $p = [x, y, z]^\top$ lies on the plane π if and only if:

$$\pi^\top \begin{bmatrix} p \\ 1 \end{bmatrix} = \pi^\top \tilde{p} = 0. \quad (2)$$

With this constrain and given a set of noisy observed points from the same planar surface, one can solve the plane estimation mainly by two approaches. The **centered method** minimizes the overall point to plane error

$$\min_{\pi} \sum_{n=1}^N \|\eta^\top p_n + d\|^2. \quad (3)$$

The solution comes in two steps:

$$\min_{\eta} \left\{ \sum_{n=1}^N \eta^\top \underbrace{(p_n - E\{p\})}_{\Sigma_p} (p_n - E\{p\}) \eta \right\} \quad (4)$$

$$d = -E\{\eta^\top p\}, \quad (5)$$

first the eigendecomposition of the 3×3 matrix Σ_p solves the value of η and then d is obtained.

The **homogeneous method** calculates the point to plane error of a plane π without centering the data points:

$$\min_{\pi} \sum_{n=1}^N \|\pi^\top \tilde{p}_n\|^2 = \pi^\top \tilde{P} \tilde{P}^\top \pi \quad (6)$$

where the matrix \tilde{P} is the stacked vector of N homogeneous points. This arrangement of terms in the homogeneous plane estimation method allows us to define the S matrix:

$$S = \tilde{P} \tilde{P}^\top = \sum_{n=1}^N \tilde{p}_n \tilde{p}_n^\top, \quad (7)$$

which is the *Summation* of the outer product of all points in the plane, hence matrix S . The solution of (6) is calculated using the eigendecomposition of the 4×4 matrix S . In [40] there is a comparison of the two methods yielding similar results.

Our ultimate objective is the optimization of the trajectory and the geometrical features in the map. The disadvantage of the *centered method* is that every time a new sample is added or modified, all calculations should be carried out again. It is more natural to develop the *homogeneous method* to account for poses in a highly efficient solution.

Then, the Eigen-Factors is a generalization of the homogeneous plane estimation observed over a sequence of reference frames or poses $T_t \in SE(3)$ at different instants of time $t \in \{1, \dots, H\}$. It can also be understood as a trajectory $\mathbf{T} = \{T_1, \dots, T_H\}$. Each of these poses transforms points to a global reference frame g , such that gT_t , where we will omit the global frame reference for simplicity in following sections. The underlying idea is that the same plane π is observed from different poses T_t but the planar constraint must hold for all

views. Accordingly, we can reformulate the plane estimation problem for the plane π as

$$\min_{\pi} \sum_{t=1}^H \sum_{n=1}^{N_t} \|\pi^\top T_t \tilde{p}_{t,n}\|^2 = \min_{\pi} \pi^\top \left(\sum_{t=1}^H T_t S_t T_t^\top \right) \pi, \quad (8)$$

where each of the points $\tilde{p}_{t,n}$ denotes the reference frame it was observed t and the matrix S_t includes all these N_t points as in (7). By re-arranging terms one can see as the plane π is out of the summation, so the plane solution boils down to the eigendecomposition of this new matrix. Therefore, we define the variable Q as the summation

$$Q(\mathbf{T}) = \sum_{t=1}^H T_t S_t T_t^\top = \sum_{t=1}^H Q_t(T_t), \quad (9)$$

where each component Q_t depends on the matrix S_t , calculated only once, and the current 3D pose estimation T_t . The matrix S_t expresses points in the local coordinate system at time t and is constant, while the matrix Q is expressed in the global reference frame and is recalculated for each new updated trajectory.

The solution of the minimization problem is obtained directly by the eigendecomposition:

$$\begin{aligned} \pi^* &= k \cdot v_{\min}(Q(\mathbf{T})) \\ \text{s.t. } \|\eta^*\| &= 1. \end{aligned} \quad (10)$$

The minimum eigenvector v_{\min} is proportional to the plane solution. The exact solution, in order to have geometrical meaning, must fulfill the definition of a plane (1) with unit normal η . Therefore, it is multiplied by the scalar value k . Without this correction, each of the errors would be scaled differently and the solution would be biased. The summation of the point to plane squared error (for plane π) is equal to:

$$\min_{\pi} \pi^\top Q(\mathbf{T}) \pi = k^2 \lambda_{\min}(Q(\mathbf{T})) = \lambda_{\pi}(\mathbf{T}) \quad (11)$$

where λ_{\min} is the minimum eigenvalue, which equals the minimum cost or minimum error after estimation after scaling by k^2 , easily derived from (10). Note that the minimization of the plane is implicit after solving the algebraic equation by the eigendecomposition, so the plane variables can be removed from the state variables.

The function $\lambda_{\pi}(\cdot)$ obtained in (11) for the plane π shows some interesting properties. In the ideal case of no-noise, this function should be zero and its values are always positive by construction $\lambda_{\pi}(\cdot) \geq 0$. We could reformulate this as an **implicit observation function** of the form $h(x, z) = 0$, where in our particular case, the state x is the trajectory \mathbf{T} and the observation z are all points. In contrast, an explicit observation is of the form $h(x) = z$ which when optimizing tries to fit the state with the observations.

Unfortunately, this implicit observation function is not suitable for general nonlinear least squares (NLLS). We will later derive a state estimation problem from $\lambda_{\pi}(\cdot)$, where the total cost to minimize is

$$C(\mathbf{T}) = \sum_{m=1}^M \lambda_{\pi_m}(\mathbf{T}) \quad (12)$$

given that M is the total number of observed planes. Some important remarks:

- The cost $C(\mathbf{T})$ is equal to the total point-to-plane squared error evaluated for each of the poses T_t .
- The complexity is independent of the number of points, since the matrix S_t requires them to be summed only once and use thereafter without modifications.
- The plane parameters are estimated in closed form and the state variables are the sequence of poses \mathbf{T} .

This is the essence of the EF, a function that seeks to minimize the point to plane error w.r.t. the trajectory. The next sections are dedicated to the particular optimization of this function that requires specific development.

Our approach is an Alternating optimization, where the plane parameters are obtained in closed form by the eigen-decomposition and then the reduced problem is estimated by optimizing w.r.t. the trajectory \mathbf{T} . Other alternatives to the calculation of separable variables include the variable projection [41] or the general Wiberg approach [42]. We have chosen the alternating optimization due to its simplicity and efficiency, since the main purpose of EF is map refinement to improve the quality of the map.

IV. RETRACTION AND OPTIMIZATION ON THE MANIFOLD

This section introduces some tools from optimization on matrix manifolds [43] required for the correct development of a second-order optimization method for the Eigen Factors. The problem of interest is to further develop the form $Q(T) : SE(3) \rightarrow \mathbb{R}^{4 \times 4}$, so we will propose systematic rules to differentiate any function involving $SE(3)$ in a simple way.

A Rigid Body Transformation (RBT), denoted as ${}^f T_o \in SE(3)$, allows to transform points from an origin reference system o to a final reference system f . It also transforms reference frames or simply expresses a 3D pose uniquely. More formally, the Special Euclidean group is

$$SE(3) = \left\{ T = \begin{bmatrix} \mathbf{R} & \mathbf{t} \\ 0 & 1 \end{bmatrix} \mid \mathbf{R} \in SO(3) \wedge \mathbf{t} \in \mathbb{R}^3 \right\}. \quad (13)$$

In addition, RBT is a matrix group $SE(3) \subset \mathbb{R}^{4 \times 4}$ and due to its inner structure and properties is a Riemannian manifold. As such, there is a smooth mapping (chart) from a subgroup of $SE(3)$ elements to the vector space \mathbb{R}^6 . It is well known that the dimensionality of a 3D pose is six, however, there exist several possible mappings.

Our interest is on the optimization of a cost function whose input is an element of $SE(3)$ or more generally, an element of a manifold \mathcal{M} . Let the function $f(x) : \mathcal{M} \rightarrow \mathbb{R}$ be a mapping from a manifold to a real value. Then, if one applies directly the definition of directional derivative

$$\lim_{h \rightarrow 0} \frac{f(x + h\eta) - f(x)}{h}, \quad (14)$$

finds this operation not suitable for numerical calculations.

One can solve this problem by using a *retraction* mapping.

Definition 1. A retraction $R_T(\xi)$ is a smooth mapping from the tangent space around the T element to the manifold:

$$R_T(\xi) : \mathbb{R}^6 \rightarrow SE(3). \quad (15)$$

Two conditions must be satisfied: i) $R_T(0_T) = T$ and ii) local rigidity (see Ch.4 [43]).

Accordingly, we can compose a new function when using a retraction:

$$\hat{f}_T = f \circ R_T, \quad (16)$$

from the tangent space \mathbb{R}^6 to a real value. This new function \hat{f}_T admits a directional derivative (14). As a convention in this paper, all retractions are denoted with the *hat* superscript.

As a result, an optimization problem $x' = x + \Delta x$, which is not well defined for elements of a manifold $x \in \mathcal{M}$, becomes well defined when using a retraction

$$T' = R_T(\Delta\xi). \quad (17)$$

In the case of first order optimization, the update is proportional to the gradient direction $\Delta\xi = -\alpha \nabla_\xi \hat{f}_T$. Gradient descent is one of the simplest methods for optimization: it requires a direction and a magnitude. Second-order optimization methods, provide the direction of descent $\Delta\xi = -\alpha (\nabla_\xi^2 \hat{f}_T)^{-1} \nabla_\xi \hat{f}_T$. The advantage is that the Hessian already weights this descent direction, resulting in improved convergence rates.

In the particular case of $SE(3)$, its tangent space has a structure of Euclidean space. Only under these conditions, the gradient and the Hessian are well defined after using a retraction:

$$\begin{aligned} \nabla_T f(T) &= \nabla_\xi \hat{f}_T(0_T) \\ \nabla_T^2 f(T) &= \nabla_\xi^2 \hat{f}_T(0_T). \end{aligned}$$

These results are significant since they will allow to use the concept of directional derivatives (14) by simply applying real analysis into the calculation of the gradient and Hessian in Sec.V. By doing that, we will implement a second-order optimization method that have almost no need for hyper-parameters and quadratic convergence rate [44].

A. Differentiating over the Exponential Map in $SE(3)$

The exponential map is the most natural retraction choice: its definition is highly related with the concept of perturbations over $SE(3)$ which will facilitate the calculation of derivatives in the following sections. There are other options for choosing a retraction mapping, as long as they satisfy the definition.

The exponential map defines the retraction R_T in the following way:

$$R_T(\xi) = \text{Exp}(\xi)T. \quad (18)$$

We follow a left-hand-side convention, but the right-hand-side is a valid retraction and it would require a similar derivation of the terms. The retraction around the identity can be expanded by using the matrix exponential definition as a Taylor series

$$R_I(\xi) = \text{Exp}(\xi)I = I + \xi^\wedge + \frac{1}{2}(\xi^\wedge)^2 + o(|\xi|^3), \quad (19)$$

where the vector $\xi = [\theta^\top, \rho^\top]^\top = [\xi_1, \dots, \xi_6]^\top \in \mathbb{R}^6$ and the matrix

$$\xi^\wedge = \begin{bmatrix} \theta^\wedge & \rho \\ 0 & 0 \end{bmatrix} = \begin{bmatrix} 0 & -\theta_3 & \theta_2 & \rho_1 \\ \theta_3 & 0 & -\theta_1 & \rho_2 \\ -\theta_2 & \theta_1 & 0 & \rho_3 \\ 0 & 0 & 0 & 0 \end{bmatrix} \quad (20)$$

is the Lie Algebra matrix group $\mathfrak{se}(3)$ that represents the group of infinitesimal RBT around the identity. See [45], [46] for a comprehensive explanation on the topic of RBT and its Lie algebra. This matrix can be rearranged such that it has a vector space structure

$$\xi^\wedge = G_1\xi_1 + G_2\xi_2 + \dots + G_6\xi_6, \quad (21)$$

where G_i is a 4×4 matrix of the i -th generator and the basis $\mathbf{G} = \{G_i\}, \forall i = 1, \dots, 6$.

After defining the retraction map (18), the next step is to obtain the derivative of the retraction, i.e., the exponential map evaluated at the zero element.

Lemma 1. *The derivative of the exponential map with respect to one of the Lie coordinates ξ_i is its corresponding matrix generator*

$$\frac{\partial \text{Exp}(\xi)}{\partial \xi_i} = G_i. \quad (22)$$

Proof. One can expand analytically the definition of the matrix exponent in (19)

$$\begin{aligned} \frac{\partial \text{Exp}(\xi)}{\partial \xi_i} &= \frac{\partial}{\partial \xi_i} \left(I + \xi^\wedge + \frac{1}{2}(\xi^\wedge)^2 + o(|\xi|^3) \right) \Big|_{\xi_i=0} \\ &= G_i + \frac{1}{2}G_i\xi^\wedge + \frac{1}{2}\xi^\wedge G_i + \dots \Big|_{\xi_i=0} = G_i \end{aligned} \quad (23)$$

where after differentiating each of the terms, the higher order terms vanish when evaluated at $\xi_i = 0$. \square

Lemma 2. *The second derivative of the exponential with respect to the Lie coordinates ξ_i and ξ_j is*

$$\frac{\partial^2 \text{Exp}(\xi)}{\partial \xi_j \partial \xi_i} = \frac{1}{2}G_i G_j + \frac{1}{2}G_j G_i. \quad (24)$$

Proof. one can repeat the same procedure to expand analytically the second-order derivative:

$$\begin{aligned} \frac{\partial^2 \text{Exp}(\xi)}{\partial \xi_j \partial \xi_i} &= \frac{\partial^2}{\partial \xi_j \partial \xi_i} \left(I + \xi^\wedge + \frac{1}{2}(\xi^\wedge)^2 + o(|\xi|^3) \right) \Big|_{\xi=0} \\ &= \frac{\partial}{\partial \xi_j} \left(G_i + \frac{1}{2}G_i\xi^\wedge + \frac{1}{2}\xi^\wedge G_i \right) \Big|_{\xi=0} \\ &= \frac{1}{2}G_i G_j + \frac{1}{2}G_j G_i \end{aligned} \quad (25)$$

\square

This compact result is a 4×4 matrix, corresponding to each of the (i, j) elements of the Hessian. The overall tensor $\frac{\partial^2 \text{Exp}(\xi)}{\partial \xi^2}$ has dimensions $4 \times 4 \times 6 \times 6$ when considering each of its coordinates (i, j) .

The idea of retraction functions plus the first and second-order derivatives of the exponential map will be enormously useful when calculating derivatives of more complex functions, such as the matrices in the EF, as we show in the next section.

V. EIGEN-FACTORS DIFFERENTIATION

We will start by redefining the key functions, now as a retraction function (denoted by the $\hat{\cdot}$ indicator). The Q matrix in (9) was defined as a function of the trajectory \mathbf{T} . If only considering the transformation T_t at time t , then $Q = Q_t$ can be redefined as the retraction function (16) of the form $\hat{Q}_t = Q_t \circ R_{T_t} : \mathbb{R}^6 \rightarrow \mathbb{R}^{4 \times 4}$, such that

$$\hat{Q}_t(\xi_t) = \text{Exp}(\xi_t) \cdot Q_t \cdot \text{Exp}(\xi_t)^\top. \quad (26)$$

The point to plane error, defined as the $\lambda_\pi(\mathbf{T})$ in the EF derivation in (11), can be as well redefined as the retraction function

$$\hat{\lambda}_\pi(\xi_t) = \lambda_\pi \circ \hat{Q}_t : \mathbb{R}^6 \rightarrow \mathbb{R} \quad (27)$$

which is now a well defined function to calculate directional derivatives (14). One can evaluate the retraction around any other pose in a more general form $\hat{\lambda}_\pi(\xi)$, however, for the development that follows, we will use the current time index t and generalize the obtained expressions later to all the trajectory.

Now, it is necessary to propagate the gradient through the eigendecomposition.

Proposition 1. *The derivative of the eigenvalue λ_π with respect to the pose T_t equals*

$$\nabla_{\xi_t} \hat{\lambda}_\pi = \frac{\partial \hat{\lambda}_\pi}{\partial \xi_t} = \pi^\top \frac{\partial \hat{Q}_t}{\partial \xi_t} \pi. \quad (28)$$

Proof. See the analytical derivation in the Appendix A-A. \square

Accordingly, the calculation of the gradient boils down to calculate the derivative of \hat{Q}_t with respect to the tangent space around the element T_t of the manifold. We differentiate (26) such that

$$\frac{\partial \hat{Q}_t}{\partial \xi_t} = \frac{\partial \text{Exp}(\xi_t)}{\partial \xi_t} Q_t + Q_t \frac{\partial \text{Exp}(\xi_t)^\top}{\partial \xi_t}, \quad (29)$$

which is obtained by applying the product rule.

By using Lemma 1, one simply substitutes to obtain the derivative wrt the coordinate i :

$$\frac{\partial \hat{Q}_t}{\partial \xi_{t,i}} = G_i \cdot Q_t + Q_t \cdot G_i^\top, \quad (30)$$

where each of these elements is a 4×4 matrix. The gradient is then obtained after multiplying this result as in (28) which yields a scalar value; in total a 6D vector for each of the $i = 1, \dots, 6$ components.

This methodology is general for obtaining derivatives of functions wrt poses in 3D and allows to have a compact result, even when the image of this function is a matrix.

A. Eigen Factors, Hessian

The objective of this section is to obtain an analytical solution for the Hessian matrix $\nabla_{\xi_t}^2 \hat{\lambda}$. Similarly, we follow the same systematic procedure to derive the Hessian of the EF.

Proposition 2. *The Hessian of the Eigendecomposition with respect to the pose T_t is*

$$\frac{\partial^2 \hat{\lambda}_\pi}{\partial \xi_t^2} = \pi^\top \frac{\partial^2 \hat{Q}_t}{\partial \xi_t^2} \pi \quad (31)$$

$$\frac{\partial^2 \hat{\lambda}_\pi}{\partial \xi_t \partial \xi_{t'}} = 0, \quad \forall t \neq t'. \quad (32)$$

Proof. See the analytical derivation in the Appendix A-B. \square

An important property derived from Proposition 2 is that the Hessian matrix is **block diagonal**, which implies a fast calculation of the optimization iterations and a reduced complexity of the algorithm.

Now, we will derive the second derivative for the pair $(\xi_{t,i}, \xi_{t,j})$ of components of the vector ξ_t . We calculate the derivative of \hat{Q}_t in (26) twice, by using the product rule:

$$\begin{aligned} \frac{\partial^2 \hat{Q}_t}{\partial \xi_{t,j} \partial \xi_{t,i}} &= \frac{\partial}{\partial \xi_{t,j}} \left(\frac{\partial \text{Exp}(\xi_t)}{\partial \xi_{t,i}} Q_t + Q_t \frac{\partial \text{Exp}(\xi_t)^\top}{\partial \xi_{t,i}} \right) \\ &= \underbrace{\frac{\partial^2 \text{Exp}(\xi_t)}{\partial \xi_{t,j} \partial \xi_{t,i}} Q_t + \frac{\partial \text{Exp}(\xi_t)}{\partial \xi_{t,i}} \frac{\partial Q_t}{\partial \xi_{t,j}} + \frac{\partial Q_t}{\partial \xi_{t,i}} \frac{\partial \text{Exp}(\xi_t)^\top}{\partial \xi_{t,j}} + Q_t \frac{\partial^2 \text{Exp}(\xi_t)^\top}{\partial \xi_{t,j} \partial \xi_{t,i}}}_{B_{ij}^\top} \end{aligned} \quad (33)$$

Given the symmetry in $Q = Q^\top$, this expression is simplified and one has to calculate only the expression

$$B_{ij} = (G_i G_j + G_j G_i) \frac{Q_t}{2} + G_i \frac{\partial Q_t}{\partial \xi_{t,j}}, \quad (34)$$

and sum to its transpose in order to obtain the the components (i, j) of the Hessian. Note that the Hessian is symmetric as well, and only the upper-triangular elements need to be calculated.

B. Trajectory Optimization

In this section, we discuss different options for optimizing a trajectory $T = \{T_1, \dots, T_H\}$ or its corresponding set of vectors $\xi = \{\xi_1, \dots, \xi_H\}$. One can directly apply the EF gradient and Hessian at each pose in the trajectory, resulting in a the joint vector gradient

$$\frac{\partial \hat{\lambda}_\pi}{\partial \xi} = \left[\left(\pi^\top \frac{\partial Q}{\partial \xi_1} \pi \right)^\top, \dots, \left(\pi^\top \frac{\partial Q}{\partial \xi_H} \pi \right)^\top \right]_{6H \times 1}^\top. \quad (35)$$

This aggregation corresponds to the Cartesian product of the manifolds of each of the poses. In case there were not points observed from a pose, then the gradient would zero since it is not contributing to the EF cost in any mean. The same arrangement can be done for the Hessian:

$$\frac{\partial^2 \hat{\lambda}_\pi}{\partial \xi^2} = \text{diag} \left[\left(\pi^\top \frac{\partial^2 Q}{\partial \xi_1^2} \pi \right), \dots, \left(\pi^\top \frac{\partial^2 Q}{\partial \xi_H^2} \pi \right) \right]_{6H \times 6H}. \quad (36)$$

The total EF cost (12) can be redefined in terms of retraction function w.r.t. the joint vector of poses ξ

$$\hat{C}(\xi) = \sum_{m=1}^M \hat{\lambda}_{\pi_m}(\xi). \quad (37)$$

The optimal update of the joint vector of pose coordinates is solved by

$$\Delta \xi = -\alpha (\nabla_\xi^2 \hat{C})^{-1} \nabla_\xi \hat{C} \quad (38)$$

$$\nabla_\xi \hat{C} = \sum_m \frac{\partial \hat{\lambda}_{\pi_m}}{\partial \xi} \quad (39)$$

$$\nabla_\xi^2 \hat{C} = \sum_m \frac{\partial^2 \hat{\lambda}_{\pi_m}}{\partial \xi^2}. \quad (40)$$

C. Error Invariance to the Reference Frame

Planes are elements of the projective space \mathbb{P}^3 and they can be transformed from one reference frame to another, similarly to homogeneous points by RBT:

$${}^t \pi = {}^t T_g^{-\top} \cdot {}^g \pi, \quad (41)$$

where the plane ${}^g \pi$ in the global reference frame is transformed into ${}^t \pi$ in the local frame t .

If we explicitly account all reference frames in the point to plane error in (8), where the point ${}^t p$ was expressed in a local coordinate and the plane was expressed in the global coordinate g , then

$${}^g \pi^\top \cdot {}^g T_t \cdot {}^t \tilde{p} = {}^g \pi^\top \cdot {}^g \tilde{p} = {}^t \pi^\top \cdot {}^t \tilde{p}. \quad (42)$$

One can see that the error value is invariant to the choice of the reference: we could either transform both elements to the local reference frame or to the global frame. The EF development used the latter.

Not just that, but the planar constraint is fulfilled in any reference frame:

$${}^c \pi^\top \cdot {}^c \tilde{p} = ({}^c T_g^{-\top} {}^g \pi)^\top \cdot {}^c T_g {}^g \tilde{p} = {}^g \pi^\top \cdot {}^g \tilde{p}, \quad (43)$$

where the transformations cancel out for any new reference frame c .

D. Data Centering

From the last subsection, we can express the EF cost in a different reference frame by multiplying a transformation ${}^c T_g$ (for simplicity we write T_c) and its inverse, so the the error is unaltered:

$$\begin{aligned} \lambda_\pi &= \pi^\top \hat{Q} \pi = \pi^\top \underbrace{T_c^{-1} T_c}_I \cdot \hat{Q} \cdot T_c^\top \underbrace{T_c^{-\top} T_c}_{c_\pi} \pi \\ &= {}^c \pi^\top T_c \cdot \hat{Q} \cdot T_c^\top c_\pi. \end{aligned} \quad (44)$$

The solution is the well known eigendecomposition of $T_c \cdot \hat{Q} \cdot T_c^\top$. When applied to the gradient, yields

$$\frac{\partial \hat{\lambda}_\pi}{\partial \xi} = {}^c \pi^\top T_c \frac{\partial \hat{Q}}{\partial \xi} T_c^\top c_\pi. \quad (45)$$

If the error λ_π remains constant, then one can naturally ask if there is a reference frame more convenient than others to calculate the error. The matrix Q from (9) is composed of the following terms:

$$Q = \begin{bmatrix} Q_p & q \\ q^\top & N \end{bmatrix} \quad (46)$$

where there is a relation between q and the mean of all points from the plane, recall observed in the same global reference frame

$$q = \sum_t^H \sum_n^{N_t} T_t \cdot p_{t,n} = \sum_t^H q_t = N \cdot \mu. \quad (47)$$

The vector q is the summation of q_t each the average point in global coordinates. The 3×3 block Q_p is also related to the covariance

$$\Sigma_p \cdot N = Q_p - \frac{1}{N} q \cdot q^\top \quad (48)$$

Let the transformation matrix be a *centering data* transformation by a simple translation of the mean value:

$$T_c = \begin{bmatrix} I & -\mu \\ 0 & 1 \end{bmatrix} \quad (49)$$

In that case, the result of this transformation is

$$T_c \begin{bmatrix} Q_p & q \\ q^\top & N \end{bmatrix} T_c^\top = \begin{bmatrix} Q_p - \frac{1}{N} q \cdot q^\top & 0 \\ 0 & N \end{bmatrix}, \quad (50)$$

where top left block corresponds to the scaled covariance (48).

Alternatively, we could have asked: what is the transformation that applied to the plane π yields a d component zero? Intuitively, the higher d , the more sensible the eigendecomposition is. Then

$$\begin{bmatrix} \eta \\ d \end{bmatrix} = \begin{bmatrix} I & 0 \\ -\mu^\top & 1 \end{bmatrix} \begin{bmatrix} \eta \\ 0 \end{bmatrix}, \quad (51)$$

which is valid since we already defined $d = -E\{\eta^\top p\}$ in (5).

We will make use of this form assuming T_c is a constant. However, this is not strictly the case, since $T_c(\mathbf{T})$. In Appendix B we discuss further how the exact gradient is equal and how the Hessian is slightly different and dense, however, this component depends on the number of poses. We have decided to maintain the Hessian matrix diagonal as derived in previous sections.

In the evaluations, we will use the method just described in this section, the EF-center, which will be referred to in short as EF.

VI. EXPERIMENTS

Experiments are targeted to evaluate performance of different plane-based SLAM **back-end** approaches, formulated in the form of graph SLAM. Since the quality of the SLAM full pipeline could also be affected significantly by detection and association algorithms on the front-end, the question about quality of the full pipeline remains out of the scope of this paper and instead we focus only on the back-end. To achieve this, we consider pre-labeled data from different sensor modalities by developing our synthetic generator and using labeled data for ICL NUIM [47] and KITTI [48] sequences from EVOPS benchmark [49].

The following approaches are taken for evaluation as the main representatives of methods on graph plane-based SLAM: BAREG [29], π -Factor [22], BALM [30], [31], EigenFactor (EF, ours). BAREG, π -Factor and EigenFactor are implemented in our common framework `mrob`¹ for factor-graph optimization problems. In particular, we use a Levenberg-Marquadt optimizer with tolerance of 10^{-2} for all the methods and the exact same initial conditions. Since the BALM formulation is also graph SLAM, we consider the author's original implementation with default parameters [30].

A. Complexity Analysis

The theoretical complexity analysis is depicted in Table I. We have included three categories that are required at each iteration step of the optimization, assuming that planes are observed over the full sequence.

TABLE I: Complexity comparison of various plane SLAM methods.

	# Planes Estim.	Evaluation	Optimization
BAREG	MH	$O(HM)$	$O(H)$
π -Factor	0	$O(HM)$	$O(H^3 + M)^*$
BALM2	M	$O(HM)$	$O(H^3)$
EF	M	$O(HM)$	$O(H)$

First column is the number of planes to be estimated. For instance, π -Factor does not evaluate the planes, since they are part of their state variables. Other methods evaluate each plane once and BAREG needs to evaluate each plane at each pose in the trajectory. Second column — *evaluation* and it refers to the complexity to evaluate the residuals for each method and calculate the Jacobians and Hessian if needed. We see how all methods provide the same complexity which depends on the number of planes M and poses in the trajectory H .

Finally, the optimization complexity, and this is related to the structure of the problem. For instance BAREG and EF show linear complexity since they have a block diagonal matrix to invert. π -Factor estimates a larger state vector $H+M$ and requires to invert a sparse matrix (we show worst case) and Schur trick could be used to marginalize the plane landmarks M . BALM2 requires to invert a dense matrix, so it shows cubic complexity.

B. Synthetic planes

In order to evaluate the quality of planar-based SLAM back-end, we have developed a generator of synthetic environment with planes.

Setup. The generator provides set of point clouds with planes and reference trajectory for them, and could be parameterized by number of poses, number of planes, number of points per plane, point-to-plane noise, trajectory noise. Example of generated synthetic environment is presented in Fig. 2. The default parameters configuration is the following: number of poses — 10, number of planes — 10, number of points per plane — 50, point-to-plane noise — 0.04 meters, trajectory

¹<https://github.com/prime-slam/mrob>

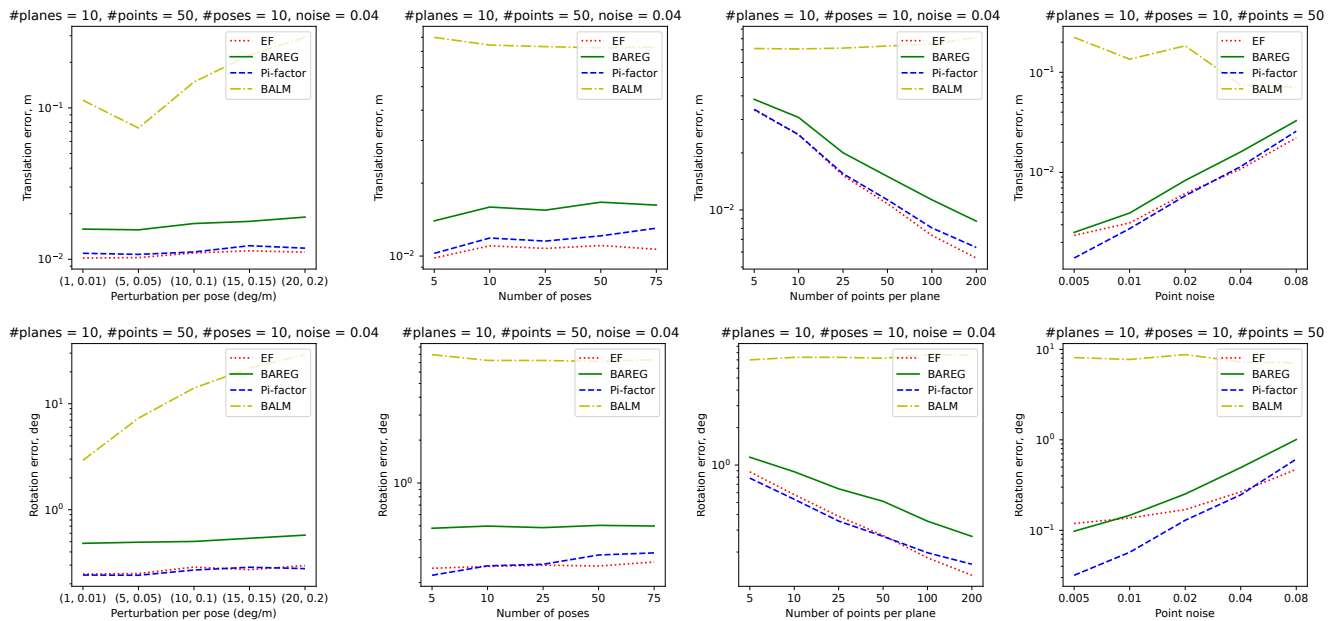


Fig. 1: Evaluation results in synthetic environments with planes swiping over such parameters as: pose perturbation, number of poses in trajectory, number of points per plane, point-to-plane noise. *Top*: RPE translation error in different simulator configurations, *Down*: RPE rotation error in different simulator configurations

perturbation per each pose — 0.05 meters and 5 degrees. In evaluation, we chose one parameter to be swiped over different values whereas other parameters remain constant. Relative Pose Error [50] is used to estimate the accuracy of methods, rotation and translation part independently.

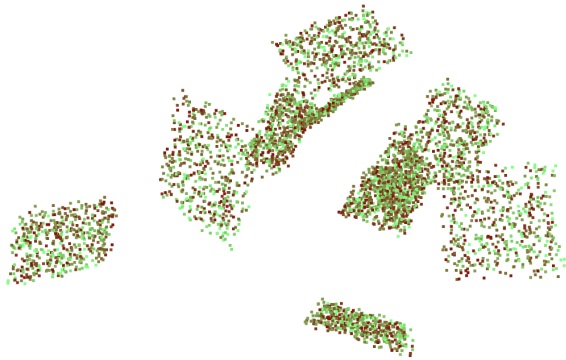


Fig. 2: Synthetic Environment. Points are generated to emulate sampling over planes.

Results and discussion Results of evaluation are depicted in Fig. 1. In general, on all parameters variations methods could be ordered as following: EF and π -Factor show almost the same quality, BAREG is on the second place, but still at a relatively small distance, and BALM diverges on huge perturbations. Since BALM pipeline is used with built-in front-end, the divergence could be explained by this fact. It is worth to note that on trajectory perturbation experiment, EF, π -Factor and BALM show consistent results on all perturbation ranges, meaning that they show good convergence and could be applied for global alignment, not only local trajectory

refinement. Swiping over such parameters as number of poses, number of points per plane, point-to-plane noise the method’s quality is ranged in the same order, but it could be noticed that in extreme conditions such as huge plane noise or amount of poses, EF shows more stable results than π -Factor.

C. RGBD

The second stage of evaluation includes quality estimation on RGBD data. Since evaluation considers only back-ends, we take RGBD sequences from the EVOPS benchmark [49] with pre-labeled planes. Benchmark has labeled data for ICL NUIM and TUM RGBD dataset. TUM RGBD has only small pieces of trajectories covered by enough amount of planes, therefore only ICL NUIM data is used.

Setup For evaluation, we randomly sample 50 different subsequences, whose length is 30 consecutive frames. For every subsequence, the poses in original trajectory are perturbed in the range from 0.001-0.15 degrees and 0.001-0.15 meters. Two configuration of ICL NUIM dataset are used: original and one that emulates Kinect noise. For evaluation, Relative Pose Error is used for translation and rotation parts independently.

Results and discussion Qualitative example of pose perturbation and later alignment by EF is depicted in Fig. 3. Since all methods give good map for visual quality assessment, only one method is chosen for visualization. Results of evaluation with metrics are presented in Fig. 4. On depth data without noise, π -Factor and BAREG show the best results, EF is the second but still with very small error and BALM shows good results only on small perturbations, whereas later diverges, that could be explained by interference with the front-end error. On data that emulates Kinect noise the situation changes — EF shows the best performance, downgrading one order with respect

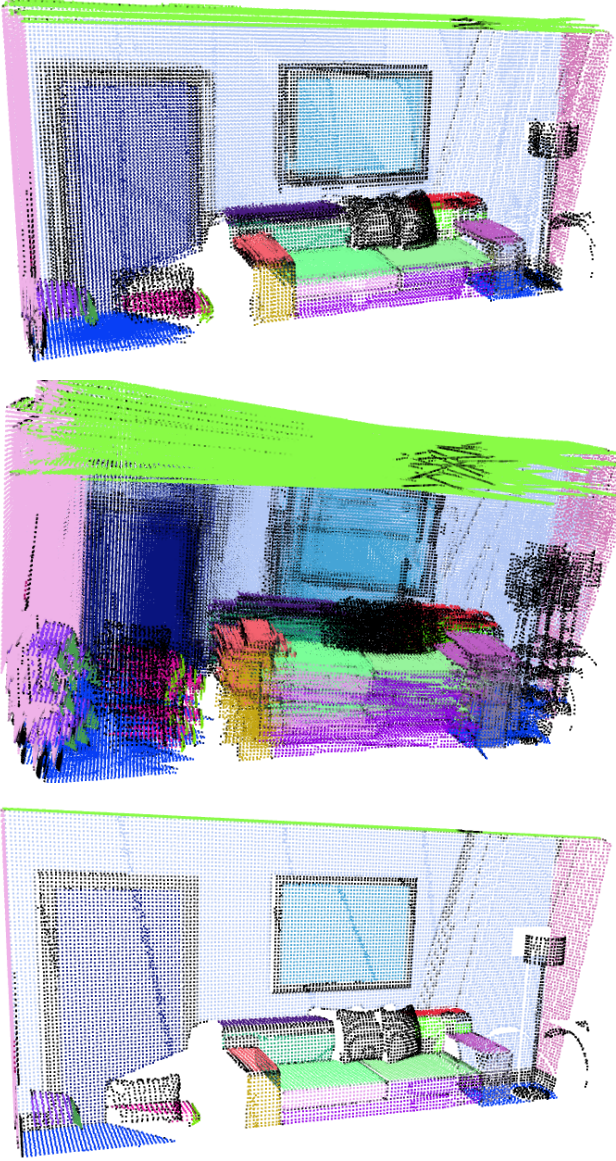


Fig. 3: *Top*: Example of the map aggregated from 10 poses with amount of noise 1 degree, 0.01 meter per pose. *Middle*: Example of map aggregated from 10 poses with amount of noise 5 degree, 0.05 meter per pose. *Down*: Result of alignment using the EF algorithm.

to data without noise, the second one result is demonstrated by π -Factor which error is two orders more than on original synthetic data, BAREG is the third one with 3 orders worse quality. The same as in previous synthetic experiments, EF, π -Factor and BAREG demonstrate almost constant error among all ranges of perturbation. To sum up, in this experiment setting EF shows more stable results when the data is close to real in comparison to other methods that degrade drastically when more noisy data is provided.

D. LiDAR

Finally, methods are evaluated on KITTI dataset with real LiDAR data.

Setup Original ground truth poses of KITTI dataset are not suitable for evaluation using classical pose-based metrics, since they provide noisy data [49]. Therefore, the following scenario is used: ground truth trajectory is used as the initial conditions for all methods, then the methods optimize over pre-labeled planes from the EVOPS benchmark. For evaluation we consider 100 submaps of length 30 poses, randomly sampled from map 00. To estimate the quality of alignment, no-reference map metrics MME [37], MPV [38] and MOM [39] are used.

Results and discussion No-reference map-metrics statistics over the methods is presented in Tab. II, BALM is not reported in the results, since it doesn't provide any convergence on those sequences. Following results, EF shows improvement of poses that gives better map quality on all metrics, qualitative demonstration of this can be found in Fig. 5. Other methods sometimes show improvement over ground truth poses, but not so drastically as EF. It is worth to note, that KITTI LiDAR data is noisy and EF shows good results even in those conditions.

TABLE II: No-reference map metrics on KITTI dataset

	MME ↓	MPV ↓	MOM ↓
BAREG	0.24	0.0276	0.0046
π -Factor	0.26	0.0275	0.0028
GT	0.23	0.0276	0.0029
EF (ours)	0.17	0.0266	0.0023

VII. CONCLUSIONS

We have presented the Eigen Factors method for back-end plane SLAM. The main contribution is on calculating exactly the point error of all points in the plane at $O(1)$ complexity when evaluating the optimization cost. We have entirely reformulated the problem, from the perspective of manifold optimization and we have derived an analytical solution for the gradient and the Hessian matrix of the EF by using a simple procedure to calculate derivatives. This derivation turns out to be very efficient for optimization, since it requires an inversion of a block diagonal matrix (Hessian). The proposed method is an alternating optimization where first the plane parameters are calculated in closed form and then a Newton-Raphson optimization is done on the resulting subproblem by considering the estimated plane variables fixed.

For the evaluations, we have compared EF with other state-of-the-art methods in back-end plane SLAM, showing solid results across synthetic and real data for RGBD and LiDAR. EF presents overall good accuracy in all domains, and excellent results for different number of poses, number of planes, point noise and initial conditions. We have also evaluated no-reference metrics for the quality of the 3D reconstruction, where EF shows superior results.

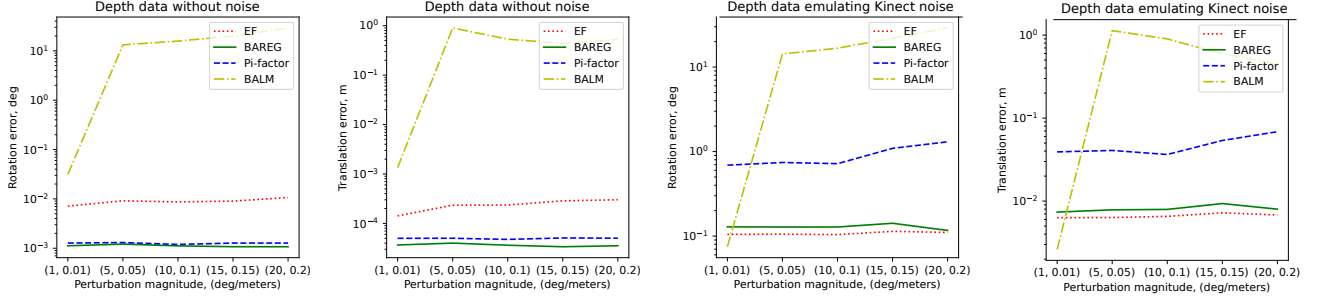


Fig. 4: *Left*: Evaluation on ICL without noise in the point cloud with respect to perturbations in the initial poses. *Right*: Evaluation adding noise to the PC.

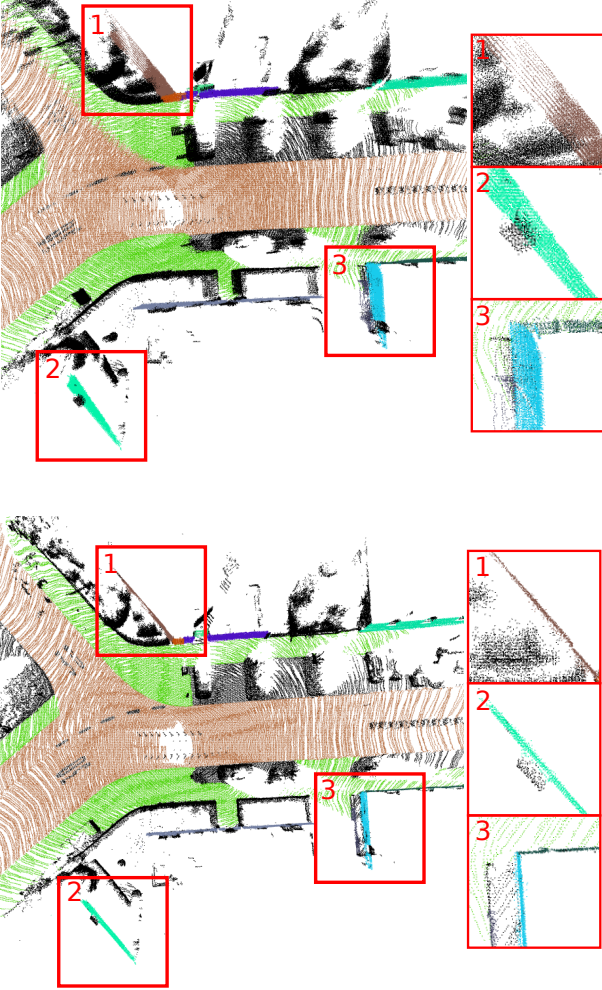


Fig. 5: *Top*: map aggregated from KITTI ground truth poses. *Down*: map aggregated from poses obtained by EF.

APPENDIX A

A. First Order Derivative over the Eigendecomposition

Proof. By definition, the eigendecomposition is expressed as $\hat{Q}v = \hat{\lambda}v$. The vector of parameters v is a unit vector s.t. $\|v\|^2 = v^\top v = 1$. One can exchange the unit vector v for any other vector $\pi \in \mathbb{P}^3$, since $\pi = kv$ and $\|\pi\| = k^2$, from definition $\hat{\lambda}_\pi$ in (11).

$\hat{Q}\pi = \hat{\lambda}\pi$ is derived wrt each of i th coordinates of the variable $\xi_{t,i}$, for simplicity it is written as ξ_i ,

$$\hat{Q} \frac{\partial \pi}{\partial \xi_i} + \frac{\partial \hat{Q}}{\partial \xi_i} \pi = \lambda \frac{\partial \pi}{\partial \xi_i} + \frac{\partial \hat{\lambda}}{\partial \xi_i} \pi \quad (52)$$

$$\text{s.t. } \pi^\top \frac{\partial \pi}{\partial \xi_i} = 0. \quad (53)$$

Taking into account that the matrix \hat{Q} is symmetric by construction, then

$$\hat{Q} = \hat{Q}^\top \implies \pi^\top \hat{Q} = \hat{\lambda} \pi^\top. \quad (54)$$

One can pre-multiply the expression (52) by π^\top , substitute (54) and do some manipulations:

$$\begin{aligned} \pi^\top \hat{Q} \frac{\partial \pi}{\partial \xi_i} + \pi^\top \frac{\partial \hat{Q}}{\partial \xi_i} \pi &= \pi^\top \hat{\lambda} \frac{\partial \pi}{\partial \xi_i} + \pi^\top \frac{\partial \hat{\lambda}}{\partial \xi_i} \pi \\ \underbrace{\hat{\lambda} \pi^\top \frac{\partial \pi}{\partial \xi_i}}_{(53)} + \pi^\top \frac{\partial \hat{Q}}{\partial \xi_i} \pi &= \underbrace{\hat{\lambda} \pi^\top \frac{\partial \pi}{\partial \xi_i}}_{(53)} + \frac{\partial \hat{\lambda}}{\partial \xi_i} \underbrace{\pi^\top \pi}_{k^2} \\ \pi^\top \frac{\partial \hat{Q}}{\partial \xi_i} \pi &= \frac{\partial \hat{\lambda} k^2}{\partial \xi_i} = \frac{\partial \hat{\lambda}_\pi}{\partial \xi_i}. \end{aligned} \quad (55)$$

Recall from (9) that $\hat{Q} = \sum \hat{Q}_\tau$, so the only derivative that is not zero is the one corresponding to the \hat{Q}_t component. One can re-arrange each of the i coordinates in ξ_t and finally write

$$\frac{\partial \hat{\lambda}_\pi}{\partial \xi_t} = \pi^\top \frac{\partial \hat{Q}_t}{\partial \xi_t} \pi. \quad (56)$$

□

B. Second Order Derivative over the Eigendecomposition

Proof. The second derivative is obtained after deriving for each component of $\xi_{t,i}$ and $\xi_{t,j}$, written as ξ_i and ξ_j

$$\frac{\partial}{\partial \xi_j} \left(\frac{\partial \hat{\lambda}_\pi}{\partial \xi_i} \right) = \frac{\partial}{\partial \xi_j} \left(\pi^\top \frac{\partial \hat{Q}_t}{\partial \xi_i} \pi \right) \quad (57)$$

$$\frac{\partial^2 \hat{\lambda}_\pi}{\partial \xi_j \partial \xi_i} = \frac{\partial \pi^\top}{\partial \xi_j} \frac{\partial \hat{Q}_t}{\partial \xi_i} \pi + \pi^\top \frac{\partial^2 \hat{Q}_t}{\partial \xi_j \partial \xi_i} \pi + \pi^\top \frac{\partial \hat{Q}_t}{\partial \xi_i} \frac{\partial \pi}{\partial \xi_j} \quad (58)$$

One can manipulate the expression in (55) by pre-multiplying it by π

$$\pi \frac{\partial \hat{\lambda}_\pi}{\partial \xi_i} = k^2 \frac{\partial \hat{Q}_t}{\partial \xi_i} \pi = \pi \frac{\partial \hat{\lambda}}{\partial \xi_i} k^2. \quad (59)$$

The constant value k^2 cancels out and this expression is substituted in (58) plus the symmetry of Q in (54)

$$\frac{\partial^2 \hat{\lambda}_\pi}{\partial \xi_j \partial \xi_i} = \underbrace{\frac{\partial \pi^\top}{\partial \xi_j} \pi}_{0} \cdot \frac{\partial \hat{\lambda}}{\partial \xi_i} + \pi^\top \frac{\partial^2 \hat{\lambda}_\pi}{\partial \xi_j \partial \xi_i} \pi + \frac{\partial \hat{\lambda}}{\partial \xi_i} \cdot \underbrace{\pi^\top \frac{\partial \pi}{\partial \xi_j}}_0 \quad (60)$$

where the first and last element vanish due to (53). Finally

$$\frac{\partial^2 \hat{\lambda}_\pi}{\partial \xi_j \partial \xi_i} = \pi^\top \frac{\partial^2 \hat{Q}_t}{\partial \xi_j \partial \xi_i} \pi. \quad (61)$$

The second condition can be easily verified by noting that the right hand side of (57) only depends on the matrix Q_t at pose t and the contribution from other poses at $t' \neq t$ vanishes after the first differentiation. \square

APPENDIX B

APPROXIMATION OF THE EF CENTER

The retraction of the centering transformation T_c for the particular pose at t can be written

$$\begin{aligned} R_{T_c}(\xi_t) &= \begin{bmatrix} I & -\mu(\xi_t) \\ 0 & 1 \end{bmatrix} = \begin{bmatrix} I & -\frac{1}{N} \left(\sum_{\tau \neq t}^H q_\tau + \text{Exp}(\xi_t) q_t \right) \\ 0 & 1 \end{bmatrix} \\ &= \begin{bmatrix} 0 & \frac{1}{N} (q_t - \text{Exp}(\xi_t) q_t) \\ 0 & 1 \end{bmatrix} T_c = \mathcal{E}(\xi_t) T_c. \end{aligned} \quad (62)$$

where we have used the results from (47). Its derivative at any pose t for the i -th coordinate

$$\frac{\partial \mathcal{E}(\xi)}{\partial \xi_i} = \begin{bmatrix} 0 & -\frac{1}{N} G_i q_t \\ 0 & 0 \end{bmatrix}. \quad (63)$$

Therefore, the total gradient starting from (45)

$$\begin{aligned} \frac{\partial}{\partial \xi_i} \left(\mathcal{E}(\xi_t) T_c \text{Exp}(\xi_t) Q \text{Exp}(\xi_t)^\top T_c^\top \mathcal{E}(\xi_t)^\top \right) &= \\ \frac{\partial \mathcal{E}(\xi)}{\partial \xi_i} T_c Q T_c^\top + T_c G_i Q_i T_c^\top + (\dots)^\top & \quad (64) \end{aligned}$$

where the first term after the equal is zero (see below) and the second term was already obtained before in (45). There are 2 more terms as a result of the differentiation, but they happen to be the transposed of the first two. We will expand the first term and evaluate its derivative after multiplying by the plane ${}^c \pi$:

$$\begin{bmatrix} \eta^\top & 0 \end{bmatrix} \begin{bmatrix} 0 & -\frac{1}{N} G_i q_t \\ 0 & 0 \end{bmatrix} \begin{bmatrix} Q_p - \frac{1}{N} q \cdot q^\top & 0 \\ 0 & N \end{bmatrix} \begin{bmatrix} \eta \\ 0 \end{bmatrix} = 0. \quad (65)$$

This expression is always zero $\forall i$, therefore it has null contribution on the gradient, so the results is exactly the same as obtained in in (45).

The Hessian will be dense since there is a term from T_c that depends on all poses and it does not cancel out as in the gradient case. One could derive it with the definition of retraction, but this term is weighted roughly by $\frac{1}{H^2}$ so its contribution diminishes fast with the number of poses.

We have tested empirically that for 2 poses, the relative difference between the exact Hessian and the approximated Hessian (as a matrix norm) is around 30% and for 20 poses, the difference is less than 1%, so its approximation is well justified.

REFERENCES

- [1] F. Dellaert and M. Kaess, "Square root SAM: Simultaneous localization and mapping via square root information smoothing," *The International Journal of Robotics Research*, vol. 25, no. 12, pp. 1181–1203, 2006.
- [2] B. Triggs, P. F. McLauchlan, R. I. Hartley, and A. W. Fitzgibbon, "Bundle adjustment—a modern synthesis," in *International workshop on vision algorithms*, 1999, pp. 298–372.
- [3] J. Weingarten and R. Siegwart, "3D SLAM using planar segments," in *IEEE/RSJ International Conference on Intelligent Robots and Systems*. IEEE, 2006, pp. 3062–3067.
- [4] A. J. Trevor, J. G. Rogers, and H. I. Christensen, "Planar surface SLAM with 3D and 2D sensors," in *2012 IEEE International Conference on Robotics and Automation*. IEEE, 2012, pp. 3041–3048.
- [5] G. Ferrer, "Eigen-Factors: Plane Estimation for Multi-Frame and Time-Continuous Point Cloud Alignment," in *IEEE/RSJ International Conference on Intelligent Robots and Systems*, 2019, pp. 1278–1284.
- [6] Y. Chen and G. Medioni, "Object modeling by registration of multiple range images," in *IEEE International Conference on Robotics and Automation*. IEEE, 1991, pp. 2724–2729.
- [7] P. J. Besl and N. D. McKay, "A method for registration of 3-D shapes," *IEEE Transactions on pattern analysis and machine intelligence*, vol. 14, no. 2, pp. 239–256, 1992.
- [8] Z. Zhang, "Iterative point matching for registration of free-form curves and surfaces," *International journal of computer vision*, vol. 13, no. 2, pp. 119–152, 1994.
- [9] S. Rusinkiewicz and M. Levoy, "Efficient variants of the ICP algorithm," in *Proceedings Third International Conference on 3-D Digital Imaging and Modeling*. IEEE, 2001, pp. 145–152.
- [10] B. K. Horn, "Closed-form solution of absolute orientation using unit quaternions," *Journal of the Optical Society of America A*, vol. 4, no. 4, pp. 629–642, 1987.
- [11] K. S. Arun, T. S. Huang, and S. D. Blostein, "Least-squares fitting of two 3-D point sets," *IEEE Transactions on pattern analysis and machine intelligence*, no. 5, pp. 698–700, 1987.
- [12] S. Umeyama, "Least-squares estimation of transformation parameters between two point patterns," *IEEE Transactions on pattern analysis and machine intelligence*, vol. 13, no. 4, pp. 376–380, 1991.
- [13] A. Censi, "An icp variant using a point-to-line metric," in *IEEE International Conference on Robotics and Automation*, 2008, pp. 19–25.
- [14] A. Segal, D. Haehnel, and S. Thrun, "Generalized-ICP," in *Robotics: science and systems*, vol. 2, no. 4, 2009.
- [15] J. Serafin and G. Grisetti, "NICP: Dense normal based point cloud registration," in *IEEE/RSJ International Conference on Intelligent Robots and Systems (IROS)*, 2015, pp. 742–749.
- [16] R. Bergevin, M. Soucy, H. Gagnon, and D. Laurendeau, "Towards a general multi-view registration technique," *IEEE Transactions on Pattern Analysis and Machine Intelligence*, vol. 18, no. 5, pp. 540–547, 1996.
- [17] K. Pulli, "Multiview registration for large data sets," in *Second international conference on 3-d digital imaging and modeling (cat. no. pr00062)*. IEEE, 1999, pp. 160–168.
- [18] M. Kaess, "Simultaneous localization and mapping with infinite planes," in *IEEE International Conference on Robotics and Automation (ICRA)*, 2015, pp. 4605–4611.
- [19] P. Geneva, K. Eickenhoff, Y. Yang, and G. Huang, "Lips: Lidar-inertial 3d plane slam," in *IEEE/RSJ International Conference on Intelligent Robots and Systems (IROS)*. IEEE, 2018, pp. 123–130.
- [20] X. Zhang, W. Wang, X. Qi, Z. Liao, and R. Wei, "Point-plane slam using supposed planes for indoor environments," *Sensors*, vol. 19, no. 17, 2019.
- [21] Y. Taguchi, Y.-D. Jian, S. Ramalingam, and C. Feng, "Point-plane SLAM for hand-held 3D sensors," in *Robotics and Automation (ICRA), 2013 IEEE International Conference on*. IEEE, 2013, pp. 5182–5189.
- [22] L. Zhou, D. Koppel, and M. Kaess, "Lidar slam with plane adjustment for indoor environment," *IEEE Robotics and Automation Letters*, vol. 6, no. 4, pp. 7073–7080, 2021.
- [23] J. Zhang and S. Singh, "Loam: Lidar odometry and mapping in real-time," in *Robotics: Science and Systems*, vol. 2, no. 9, 2014.

- [24] —, “Low-drift and real-time lidar odometry and mapping,” *Autonomous Robots*, vol. 41, no. 2, pp. 401–416, 2017.
- [25] H. Ye, Y. Chen, and M. Liu, “Tightly coupled 3d lidar inertial odometry and mapping,” in *International Conference on Robotics and Automation (ICRA)*. IEEE, 2019, pp. 3144–3150.
- [26] T. Whelan, R. F. Salas-Moreno, B. Glocker, A. J. Davison, and S. Leutenegger, “Elasticfusion: Real-time dense slam and light source estimation,” *The International Journal of Robotics Research*, vol. 35, no. 14, pp. 1697–1716, 2016.
- [27] J. Behley and C. Stachniss, “Efficient Surfel-Based SLAM using 3D Laser Range Data in Urban Environments,” in *Robotics: Science and Systems*, 2018.
- [28] L. Zhou, S. Wang, and M. Kaess, “ π -lsam: Lidar smoothing and mapping with planes,” in *2021 IEEE International Conference on Robotics and Automation (ICRA)*. IEEE, 2021, pp. 5751–5757.
- [29] H. Huang, Y. Sun, J. Wu, J. Jiao, X. Hu, L. Zheng, L. Wang, and M. Liur, “On bundle adjustment for multiview point cloud registration,” *IEEE Robotics and Automation Letters (RAL)*, vol. 6, no. 4, pp. 8269–8276, 2021.
- [30] Z. Liu, X. Liu, and F. Zhang, “Efficient and consistent bundle adjustment on lidar point clouds,” *arXiv preprint arXiv:2209.08854*, 2022.
- [31] Z. Liu and F. Zhang, “BALM: Bundle adjustment for lidar mapping,” *IEEE Robotics and Automation Letters*, vol. 6, no. 2, pp. 3184–3191, 2021.
- [32] D. Tian, H. Ochimizu, C. Feng, R. Cohen, and A. Vetro, “Geometric distortion metrics for point cloud compression,” in *IEEE International Conference on Image Processing (ICIP)*, 2017, pp. 3460–3464.
- [33] E. Alexiou and T. Ebrahimi, “Point cloud quality assessment metric based on angular similarity,” in *2018 IEEE International Conference on Multimedia and Expo (ICME)*, 2018, pp. 1–6.
- [34] E. M. Torlig, E. Alexiou, T. A. Fonseca, R. L. de Queiroz, and T. Ebrahimi, “A novel methodology for quality assessment of voxelized point clouds,” in *Applications of Digital Image Processing XLI*, A. G. Tescher, Ed., vol. 10752, International Society for Optics and Photonics. SPIE, 2018, pp. 174–190. [Online]. Available: <https://doi.org/10.1117/12.2322741>
- [35] G. Meynet, J. Digne, and G. Lavoué, “PC-MSDM: A quality metric for 3d point clouds,” in *Eleventh International Conference on Quality of Multimedia Experience (QoMEX)*, 2019, pp. 1–3.
- [36] E. Alexiou and T. Ebrahimi, “Towards a point cloud structural similarity metric,” in *2020 IEEE International Conference on Multimedia Expo Workshops (ICMEW)*, 2020, pp. 1–6.
- [37] D. Droschel, J. Stückler, and S. Behnke, “Local multi-resolution representation for 6d motion estimation and mapping with a continuously rotating 3d laser scanner,” in *IEEE International Conference on Robotics and Automation (ICRA)*, 2014, pp. 5221–5226.
- [38] J. Razlaw, D. Droschel, D. Holz, and S. Behnke, “Evaluation of registration methods for sparse 3d laser scans,” in *European Conference on Mobile Robots (ECMR)*, 2015, pp. 1–7.
- [39] A. Kornilova and G. Ferrer, “Be your own benchmark: No-reference trajectory metric on registered point clouds,” in *European Conference on Mobile Robotics (ECMR)*, 2021.
- [40] K. Klasing, D. Althoff, D. Wollherr, and M. Buss, “Comparison of surface normal estimation methods for range sensing applications,” in *IEEE International Conference on Robotics and Automation*, 2009, pp. 3206–3211.
- [41] G. Golub and V. Pereyra, “Separable nonlinear least squares: the variable projection method and its applications,” *Inverse problems*, vol. 19, no. 2, p. R1, 2003.
- [42] D. Strelow, “General and nested Wiberg minimization: L2 and maximum likelihood,” in *European Conference on Computer Vision (ECCV)*. Springer, 2012, pp. 195–207.
- [43] P.-A. Absil, R. Mahony, and R. Sepulchre, *Optimization algorithms on matrix manifolds*. Princeton University Press, 2009.
- [44] J. Nocedal and S. Wright, *Numerical optimization*. Springer Science & Business Media, 2006.
- [45] K. M. Lynch and F. C. Park, *Modern Robotics*. Cambridge University Press, 2017.
- [46] J. Sola, J. Deray, and D. Atchuthan, “A micro lie theory for state estimation in robotics,” *arXiv preprint arXiv:1812.01537*, 2018.
- [47] A. Handa, T. Whelan, J. McDonald, and A. J. Davison, “A benchmark for rgb-d visual odometry, 3d reconstruction and slam,” in *2014 IEEE international conference on Robotics and automation (ICRA)*. IEEE, 2014, pp. 1524–1531.
- [48] A. Geiger, P. Lenz, C. Stiller, and R. Urtasun, “Vision meets robotics: The kitti dataset,” *The International Journal of Robotics Research*, vol. 32, no. 11, pp. 1231–1237, 2013.
- [49] A. Kornilova, D. Iarosh, D. Kukushkin, N. Goncharov, P. Mokeev, S. A., and G. Ferrer, “EVOPS Benchmark: Evaluation of Plane Segmentation from RGBD and LiDAR Data,” in *IEEE/RSJ International Conference on Intelligent Robots and Systems (IROS)*, 2022.
- [50] R. Kümmerle, B. Steder, C. Dornhege, M. Ruhnke, G. Grisetti, C. Stachniss, and A. Kleiner, “On measuring the accuracy of slam algorithms,” *Autonomous Robots*, vol. 27, no. 4, pp. 387–407, 2009.